Sensors and Materials, Vol. 35, No. 10 (2023) 3743–3761
MYU Tokyo

S & M 3448

1D Convolutional Neural Network-based Chlorophyll-a Retrieval Algorithm for Sentinel-2 MultiSpectral Instrument in Various Trophic States

Muhammad Salah,[1] Hiroto Higa,[2] Joji Ishizaka,[3] and Salem Ibrahim Salem[4,5*]

[1]Graduate School of Engineering, Kyoto University of Advanced Science,
18 Gotanda-cho, Yamanouchi, Ukyo-ku, Kyoto-shi, Kyoto 615-8577, Japan
[2]Institute of Urban Innovation, Yokohama National University,
79-5 Tokiwadai, Hodogaya-ku, Yokohama 240-8501, Japan
[3]Institute for Space-Earth Environmental Research, Nagoya University,
Furo-cho, Chikusa-ku, Nagoya 464-8601, Japan
[4]Faculty of Engineering, Kyoto University of Advanced Science,
18 Gotanda-cho, Yamanouchi, Ukyo-ku, Kyoto-shi, Kyoto 615-8577, Japan
[5]Faculty of Engineering, Alexandria University,
Lotfy El-Sied st. off Gamal Abd El-Naser - Alexandria, Alexandria Governorate 11432, Egypt

(Received January 20, 2023; accepted September 28, 2023)

Keywords: chlorophyll-a, Sentinel-2, MultiSpectral Instrument, deep learning, convolutional neural network, ocean color

Despite extensive research on chlorophyll-a (Chla) concentration retrieval methods from remote sensing reflectance (Rrs, sr^{-1}) data, there remains a need for more reliable Chla retrieval techniques. In this study, we introduce a deep learning approach based on a 1D convolutional neural network (1D CNN) architecture. In addition, we provide a new method of representing the Rrs as a sequential vector. The model architecture targets the Sentinel-2 MultiSpectral Instrument (MSI) sensor. The proposed model was trained and tested on simulated and *in situ* data collected from broad trophic states in Japan and Vietnam waters with Chla concentrations ranging from 0.02 to 148.26 mg/m^3. The proposed model was evaluated against well-accepted state-of-the-art methods: ocean color three-band (OC3), ocean color index (OCI), two-band ratio, Blend, and a neural network model with a mixture density network. The evaluation shows that the proposed method outperforms other methods with a 7.48–38.02% reduction in root mean squared error (*RMSE*) and an 11.50–39.17% lower mean absolute error (*MAE*) than the other methods. The promising performance of the proposed model suggests that more attention should be paid to the domain of sequence modeling for Rrs and the architecture of 1D CNN.

1. Introduction

Chlorophyll-a (Chla) concentration has been used as a direct indicator of the trophic state of water bodies.(1) It is also used as a representative of harmful algal blooms,(2) which makes

*Corresponding author: e-mail: salem.ibrahim@kuas.ac.jp
https://doi.org/10.18494/SAM4331

ISSN 0914-4935
https://myukk.org/

measuring Chla in water bodies a vital task to determine the quality, productivity, and environmental situation of water.

Various methods have been used to measure and retrieve Chla concentrations in water bodies,[3] which can be divided into *in situ* measurements and remote sensing methods. Remote sensing methods provide an advantage over the complexity of *in situ* methods and labor-intensive techniques involved in field measurements. However, remote sensing for Chla estimation is prone to errors and failures caused by several reasons, including cloud coverage, atmospheric correction, and the optical complexity of water.[4] Therefore, the estimation of Chla in water using remote sensing methods is a challenging task.

The estimation of Chla using satellite imagery has been widely explored owing to the accessibility of monitoring methods, and several empirical algorithms have been developed for this purpose. The majority of the currently used Chla retrieval algorithms are empirical algorithms that use the relationships between various remote sensing reflectance (Rrs) values at various bands to infer the corresponding Chla value. Band selection mainly relies on absorption peaks of the phytoplankton using Rrs to directly estimate Chla, such as the band ratio between the NIR or the red edge and the red bands,[5,6] or the ratio between the green and blue bands.[7] Ocean color (OCx) algorithms are fourth-order polynomial equations with different versions.[7–9] The selected version of the OCx algorithm depends on the target sensor, selected bands (i.e., two to six bands), and polynomial coefficients. The color index (CI) algorithm, which was developed for case 1 water where Chla < 0.25 mg/m^3, is used by the NASA Ocean Biology Processing Group (OBPG; https://oceancolor.gsfc.nasa.gov) along with OCx as a blend algorithm.[10] However, blue and green algorithms are known to overestimate Chla concentrations in inland and coastal waters, and red and NIR algorithms have been developed specifically for use in these types of water.[11] The two-band ratio algorithm uses the linear relationship between the NIR or red edge and red bands.[11] Other algorithms were developed by mixing different algorithms for more generalized solutions for case 1 and case 2 waters.[12] The previous algorithms mainly lack generalization to different water characteristics as stated above, which makes it difficult to use in all situations. Moreover, the lack of classification algorithms that can be used to determine the water type and which algorithm should be used forces the use of a single algorithm for all water cases.

On the other hand, some studies have considered using different machine learning techniques, such as support vector machines,[13–16] K-nearest neighbors,[14,16] and random forest,[14,16,17] to provide more accurate Chla estimations for specific regions. In addition to traditional machine learning methods, deep learning has attracted significant attention for water quality monitoring and remote sensing. Few researchers have used deep learning methods to estimate Chla from Rrs, such as feedforward neural networks,[18,19] which are multilayered neural networks used as regression models and trained using the backpropagation algorithm. Convolutional neural networks[20] operate on an image level instead of a pixel level, similar to other deep learning techniques, and they consist of multiple filters that are also trained using the backpropagation algorithm. The use of mixture density networks (MDNs) is a recent approach for estimating the distribution of Chla[21–23] by estimating multiple Gaussian distributions and combining them; they are basically feed-forward networks, but instead of estimating Chla directly, they try to

estimate the parameters of several Gaussian distributions that can represent Chla. Although some of the previously proposed deep learning models have shown some acceptable efficiency in determining Chla concentration, a huge room for improvement exists when considering more complex deep learning structures and when transforming the problem into other domains that can improve the efficiency of retrieval.

In this study, we consider a novel approach by treating Rrs as a sequence of reflectance values that are related to each other instead of dealing with each band as a stand-alone value; on the basis of this assumption, different sequence modeling techniques can be applied to determine Chla from Rrs by modeling the sequence of Rrs bands and encoding it into the corresponding Chla value. The method selected for this research uses 1D convolutional neural networks (1D CNNs), which were first used to analyze and classify electrocardiography (ECG) signals.[24] To the best of our knowledge, this is the first study to use 1D CNNs to model satellite data. First, we built a new model based on the 1D CNN architecture to estimate Chla concentrations in aquatic environments using MultiSpectral Instrument (MSI) sensors by considering Rrs as a sequence of related values. Next, we compared the proposed method with existing state-of-the-art algorithms using both *in situ* and simulated datasets representing a wide range of trophic states.

2. Materials and Methods

2.1 Datasets

The datasets used for developing this model are a combination of *in situ* and simulated hyperspectral data. The *in situ* dataset contains radiometric and biogeochemical measurements from various water bodies around Japan, Thailand, and Vietnam, with diverse Chla concentrations. Rrs measurements within the range of 350–900 nm were carried out using three TriOS-RAMSES hyperspectral radiometers. These instruments have a spectral interval of 2 nm and a field of view of 7 deg. Concurrently, Chla concentrations were determined using a Turner Designs 10-AU fluorometer. The procedure involved filtering 20 mL of water samples through 25 mm Whatman GF/F filters with a pore size of 0.7 μm. Subsequently, the pigments were extracted by immersing the filter in 6 mL of *N*, *N*-dimethylformamide (DMF) and storing it in a dark place at 4 °C for 4 h.[25] The locations of the sampling points are shown in Fig. 1, except for the locations of the data points from the Gulf of Thailand because such locations could not be verified. The simulated dataset is part of the CoastColour Round Robin dataset that includes simulated measurements of hyperspectral Rrs and corresponding Chla concentrations.[26]

The data used to create the generalized global Chla model included both *in situ* and simulated data. The *in situ* data consisted of 958 samples collected from seven different water bodies, which were divided into 660 training samples and 298 test samples (Table 1). The Rrs spectra of the *in situ* dataset are shown in Fig. 2. The simulated data included 5000 samples, which were randomly split into 159 training samples and 4841 test samples. The use of a small number of simulated data points was intentional to introduce randomness to the model training without negatively impacting its performance on the *in situ* data. The histogram distribution shown in Fig. 3 and the descriptive statistics in Table 1 demonstrate the variations in the characteristics of

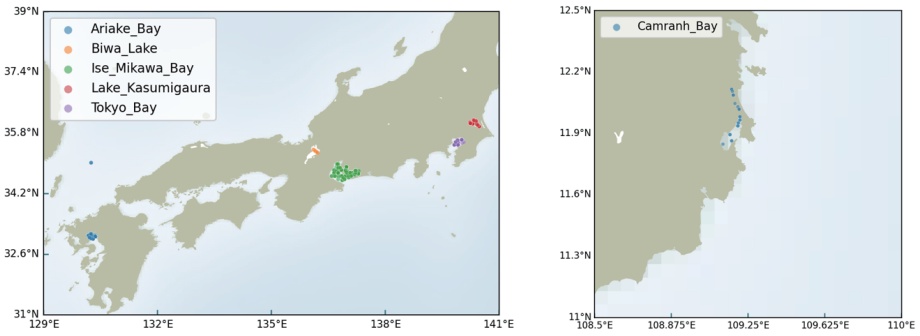

(a) (b)

Fig. 1. (Color online) Geographical distribution of the *in situ* measurements from different water bodies in (a) Japan and (b) Camranh Bay, Vietnam.

Table 1
Descriptive statistics of *in situ* and simulated Chla concentrations. The statistics include the minimum (Min), maximum (Max), mean, standard deviation (Std.), and size of the data.

Data type	site	Train/Test	Min	Max	Mean	Std.	Size
In situ	Ariake Bay	Train	2.91	39.97	16.09	10.66	57
		Test	1.53	37.50	15.44	11.09	18
	Biwa Lake	Train	0.60	1.70	0.86	0.42	5
		Test	0.63	0.63	0.63	0.00	1
	Camranh Bay	Train	1.63	52.00	8.16	10.54	20
		Test	0.81	7.86	3.19	1.95	10
	Gulf of Thailand	Train	3.05	39.79	14.21	11.17	21
		Test	5.12	37.63	12.37	10.28	8
	Ise-Mikawa Bay	Train	0.39	148.26	19.24	22.50	457
		Test	0.53	131.74	19.55	22.60	218
	Lake Kasumigaura	Train	13.16	127.34	51.72	25.92	55
		Test	21.63	94.49	48.72	18.60	22
	Tokyo Bay	Train	0.91	80.23	20.02	18.19	45
		Test	0.76	97.32	26.45	25.04	21
Simulated		Train	0.22	60.78	6.16	7.92	159
		Test	0.02	129.08	6.15	10.06	4841

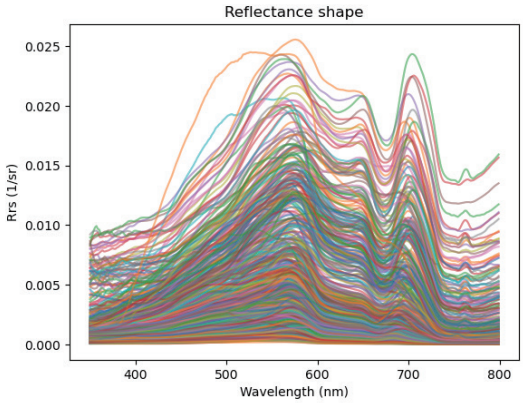

Fig. 2. (Color online) Rrs spectra of *in situ* measurements.

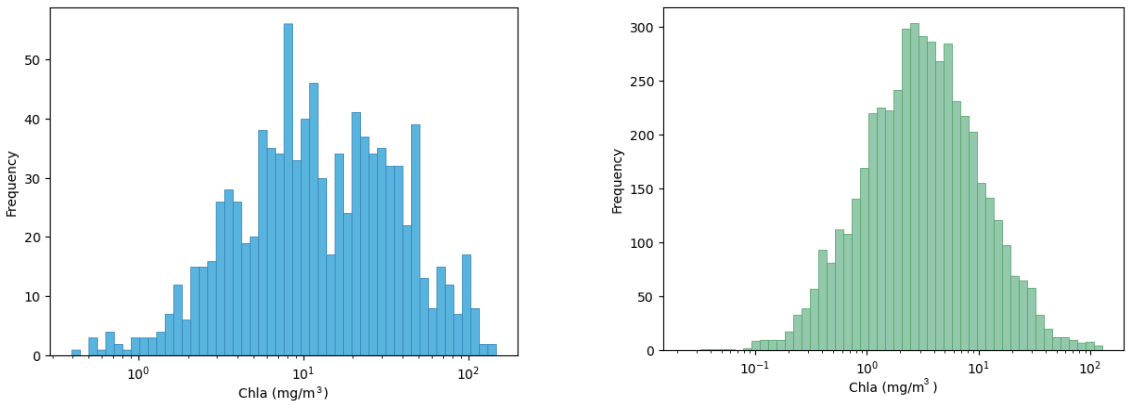

(a) (b)

Fig. 3. (Color online) Histogram distributions of (a) *in situ* and (b) simulated Chla concentrations.

the water bodies and data samples, which facilitate the development of a generalized global Chla model.

The target sensor of this study is the MSI onboard the Sentinel-2 satellite, which measures the reflectance at 13 different wavelengths, ranging from the visible and near-infrared regions to the shortwave infrared region.[27] MSI bands in the visible and NIR regions (Table 2) were considered as inputs for the 1D CNN model. The hyperspectral Rrs values of the *in situ* and simulated datasets were resampled to the MSI sensor for the training and testing of the evaluated algorithms by using the nominal bands.

2.2 Model development

The measured Rrs at each station is a sequential data vector with dependences and relationships between its values. To model the sequential data, a 1D CNN was adopted to analyze and detect different relationships and dependences between the different Rrs bands.

1D CNNs are effective deep learning models for sequential data processing, such as audio signals, time-series data, and natural language text.[28] One key advantage of 1D CNNs is their ability to learn local patterns within the input data while preserving the overall structure and context of the input. This is accomplished using the convolutional kernels shown in Fig. 4, which are small weight matrices that are applied to a sliding window of the input data, extracting local features, and combining them to form higher-level representations. 1D CNNs can be stacked to create deeper networks, which can further improve their ability to learn more complex and abstract patterns within the data.

2.2.1 Feature engineering

The input to the proposed model is Rrs in sr^{-1}, which consists of the first seven spectral bands from the Sentinel-2 MSI sensor, and the output is the Chla concentration in mg/m^3, which

Table 2
Sentinel-2 MultiSpectral Instrument (MSI) bands in the visible and near-infrared regions.

Band	Nominal wavelength (nm)	Spatial resolution (m)
1	443	60
2	490	10
3	560	10
4	665	10
5	705	20
6	740	20
7	783	20

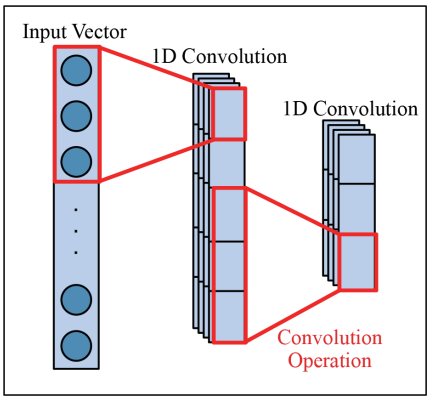

Fig. 4. (Color online) Simple 1D CNN architecture with two convolutional layers.

creates a regression problem. Various feature engineering techniques were applied to the data before they were fed to the deep learning model to facilitate the learning progress and generalization of the model.

First, an Isolation Forest anomaly detection algorithm[29] was used to ensure that all data samples do not include outliers. This algorithm is based on an isolation tree, which is constructed by randomly selecting a feature, splitting a value, and partitioning the data into two subsets. This process is recursively repeated until each data point is isolated from its leaf node. After building multiple isolation trees using different subsets of the data and measuring the average path length of the trees, data points that required fewer splits to be isolated in the tree were considered more anomalous than data points that required more splits to be isolated in the tree. The algorithm then generates an anomaly score for each data point based on its isolation in the tree, and the data points with high scores are identified as anomalies. The threshold for considering a sample as an anomaly is set to 0.55.

The Rrs values range from 4.27 e^{-6} to 2.49 e^{-2} sr^{-1} (Fig. 2), which is a massive range for deep learning. Hence, a log transformation was applied to the inputs as a technique to minimize the input range, which helps the model better represent the data and generalize for different Rrs values. Applying the log transformation to the reflectance data narrows the input range to −12.36–−3.69.

2.2.2 Model architecture

The architecture of the proposed model is shown in Fig. 5. The model construction can be described in three steps. First, feature engineering and normalization were applied to the Rrs data to produce a normalized input. Second, the output from the first step was fed to two-layered 1D CNNs that can be considered as the encoding part of the model, which captures the relationship between the input reflectance and the output Chla, and encodes the input values to an intermediate vector representation of Chla. Finally, the vector is fed to a two-layered fully connected feed-forward network with an output layer that attempts to estimate the Chla concentration for the corresponding Rrs values.

Different hyperparameters were tuned to obtain the current structure and parameters of the proposed model. The hyperparameters include the number of layers for both the CNN and the fully connected network, kernel size, the number of filters for the CNN layers, and the number of units in each of the fully connected layers. Beyond the architectural parameters, feature engineering parameters were also carefully adjusted. This involved setting the anomaly threshold to 0.55 for the Isolation Forest anomaly detection algorithm and selecting a logarithmic transformation as the normalization technique for Rrs. Figure 5 shows the different hyperparameters used for each layer in the deep learning model.

2.3. Comparison with other Chla algorithms

The performance of the proposed model was evaluated using state-of-the-art algorithms. Six well-known standard algorithms used for Chla estimation were selected for comparison: the three-band version of OC3;[8] the OCI algorithm that blends the CI algorithm with the OC3 algorithm;[10] the two-band ratio algorithm (2 Band), which indicates that the ratio of the near 705 nm band to the near 675 band is directly related to the Chla ratio;[5] the three-band ratio algorithm (3 Band), which uses the spectral bands 665, 705, and 740;[30] the four-band ratio algorithm (4 Band) using the relationship among the 560, 665, 705, and 740 bands to estimate Chla;[31] and the blend algorithm that blends the OC3 algorithm with the two-band algorithm.[12] For the band ratio algorithms, the relationship between the band ratios and the Chla value was linear. The equations and tuned parameters for the six algorithms are presented in Appendix A.

In addition to the six classical algorithms, the state-of-the-art deep learning model proposed by Pahlevan *et al.*, which is based on the MDN architecture to estimate the distribution of Chla using several Gaussian distributions, was also included in the comparison.[23]

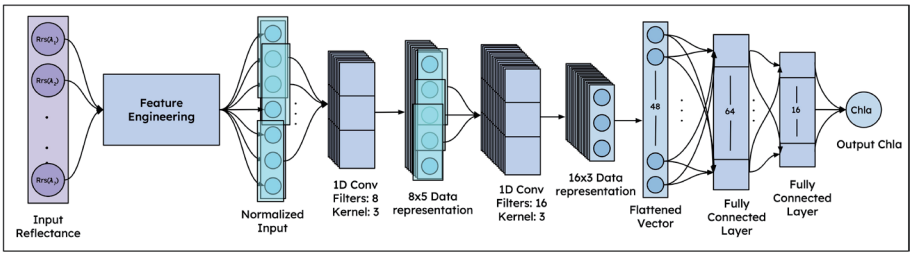

Fig. 5. (Color online) Schematic diagram illustrating the overall architecture of the proposed 1D CNN, including the feature engineering step followed by the deep learning model's main components.

2.4 Evaluation metrics

The evaluation metrics used in this study were the root mean squared error (*RMSE*), mean absolute error (*MAE*), mean absolute percentage error (*MAPE*), and *BIAS*. The proposed model, state-of-the-art deep learning model, and six standard algorithms were evaluated using the same test data. All four evaluation metrics were calculated for each model's prediction against the *in situ* measurements of Chla for comparison.

$$RMSE = \sqrt{\sum_1^n \frac{\left(\hat{y}_i - y_i\right)^2}{n}} \tag{1}$$

$$MAE = \frac{1}{n}\sum_1^n \left|\hat{y}_i - y_i\right| \tag{2}$$

$$MAPE = \frac{100\%}{n}\sum_1^n \left|\frac{\hat{y}_i - y_i}{y_i}\right| \tag{3}$$

$$BIAS = \frac{1}{n}\sum_1^n \left(y_i - \hat{y}_i\right) \tag{4}$$

Here, y_i and $\hat{y}_i$ represent the measured and model retrieved Chla values, respectively, and n refers to the number of samples.

3. Results and Discussion

The inclusion of simulated data in our study seeks to address the inherent limitations posed by the relatively small number of *in situ* Rrs–Chla pairs, allowing for the exploration of Chla distributions not fully captured by *in situ* data alone. To evaluate the efficacy of this approach, we first compared the performance characteristics of the 1D CNN model trained with and without the inclusion of 159 simulated samples. As illustrated in Fig. 6, the performance results derived from *in situ* data were similar, with a slight improvement observed in the nonsimulated data scenario, indicating that the inclusion of simulated data does not significantly affect the model's performance on *in situ* data.

In contrast, a marked change in performance was observed when assessing the model's ability to handle simulated data. The 1D CNN model, when trained exclusively on *in situ* data, showed a significant performance decrease when tested against simulated data, as demonstrated by a 100% increase in *RMSE* and 7-fold and 20-fold decreases in *MAE* and *BIAS*, respectively, as demonstrated in Fig. 6.

We further assessed the quantity of simulated data incorporated into the 1D CNN model. While a small portion of simulated data significantly enhances the model's performance on simulated data, expanding this simulated dataset negatively impacted the performance on *in situ*

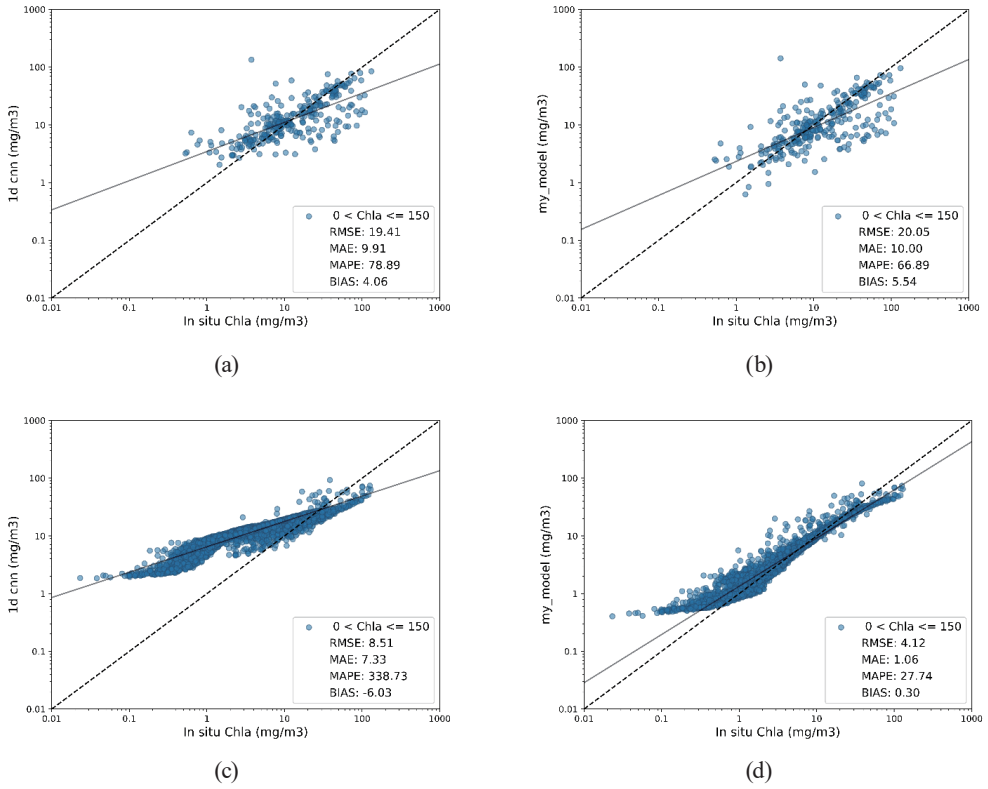

Fig. 6. (Color online) Evaluation of model performance based on training scenarios: (a) & (b) Model performance characteristics on *in situ* data, trained using *in situ* data only, and both *in situ* and simulated data, respectively. (c) & (d) Model performance characteristics on simulated data, trained using only *in situ*, and both *in situ* and simulated data, respectively.

data. Accordingly, we infer that our selected mix of *in situ* and simulated data optimizes the 1D CNN model's capacity to capture the variability present in both *in situ* and simulated distributions.

We further investigated the proposed 1D CNN's performance for Chla retrieval by comparing it with those of six standard algorithms [i.e., OC3, OCI, 2 Band, 3 Band, 4 Band, and Blend (2 Band & OC3)] and the MDN model. The models were evaluated using *in situ* and simulated datasets as discussed in the subsequent sections.

3.1 Performance evaluation based on simulated data

The performance of all models was evaluated using a simulated dataset with 4841 samples. The evaluation metrics, including *RMSE*, *MAE*, and *MAPE*, were calculated for each model on the basis of the estimated Chla values and the Chla values associated with the simulated Rrs. The overall performance of the evaluated models, shown in Table 4, indicates that the proposed model outperforms other models with a 40.97–73.74% improvement in *RMSE*. In addition, *MAE* and *MAPE* indicated that Chla retrieval was improved by at least two folds. The statistics

Table 4
Overall evaluation for all models based on the simulated test dataset.

Model	*RMSE*	*MAE*	*MAPE*	*BIAS*
Proposed Model	**4.12**	**1.06**	**27.74**	0.30
MDN	6.98	3.28	68.93	**0.25**
OC3	10.72	5.76	141.41	−3.32
OCI	10.72	5.76	141.36	−3.29
2 Band Ratio	8.10	6.77	468.26	−5.41
3 Band Ratio	15.69	14.24	1146.05	−12.04
4 Band Ratio	14.64	12.65	1011.27	−9.75
Blend (2 Band & OC3)	9.25	5.36	140.19	−3.47

tabulated in Table 4 using the simulated dataset indicate that the MDN model provides the least *BIAS* (0.25; compared with 0.30 for the proposed model). Among the standard algorithms, 2 Band and Blend are the most accurate, whereas 3 Band and 4 Band have the least retrieval accuracy with a *MAPE* of up to 1146%.

Figure 7 shows the scatterplots of the top-performing standard algorithms, along with the MDN and proposed models. The scatterplots indicate that Blend and the MDN model better model Chla in the range of 0.01–0.2 mg/m^3; however, the proposed model provides better agreement for Chla > 1 mg/m^3. Table 5 shows a detailed comparison between the different models in different Chla ranges, which clearly shows that the proposed model outperforms the other models in all evaluation metrics across all Chla ranges by multiple folds. Even though the proposed model fails to capture the very low Chla values (less than 0.2 mg/m^3), the model still performs very well in the 0–5 mg/m^3 range with a 76.97–87.18% reduction in *RMSE* compared with other models and a 78.53–89.24% reduction in *MAE*.

3.2 Performance evaluation based on *in situ* data

The performance characteristics of various models, including the proposed model, were evaluated using 298 samples of *in situ*-measured Rrs and Chla pairs. The same evaluation procedures used for the simulated data were applied to the *in situ* data, and the results are presented in Table 6, which compares the overall performance characteristics of all the models considered in this study. The results indicate a significant improvement over the standard algorithms and the MDN model, with a 7.48–38.02% reduction in *RMSE* and an 11.50–39.17% improvement in *MAE*. *MAPE* was also reduced significantly. Figure 8 shows the scatterplots of the top-performing models, which demonstrate that the scatter points are close to the unity line compared with the other algorithms.

Table 7 shows the proposed Chla retrieval model with the other algorithms for various Chla ranges. For Chla values between 0 and 5 mg/m^3, the MDN model performed slightly better than the proposed model, with lower *RMSE* and *MAE* values. Both deep-learning-based algorithms significantly outperformed the standard algorithms in this range. When considering the range of 5–10 mg/m^3, the proposed model outperforms the other algorithms, with a 15.98–31.26%

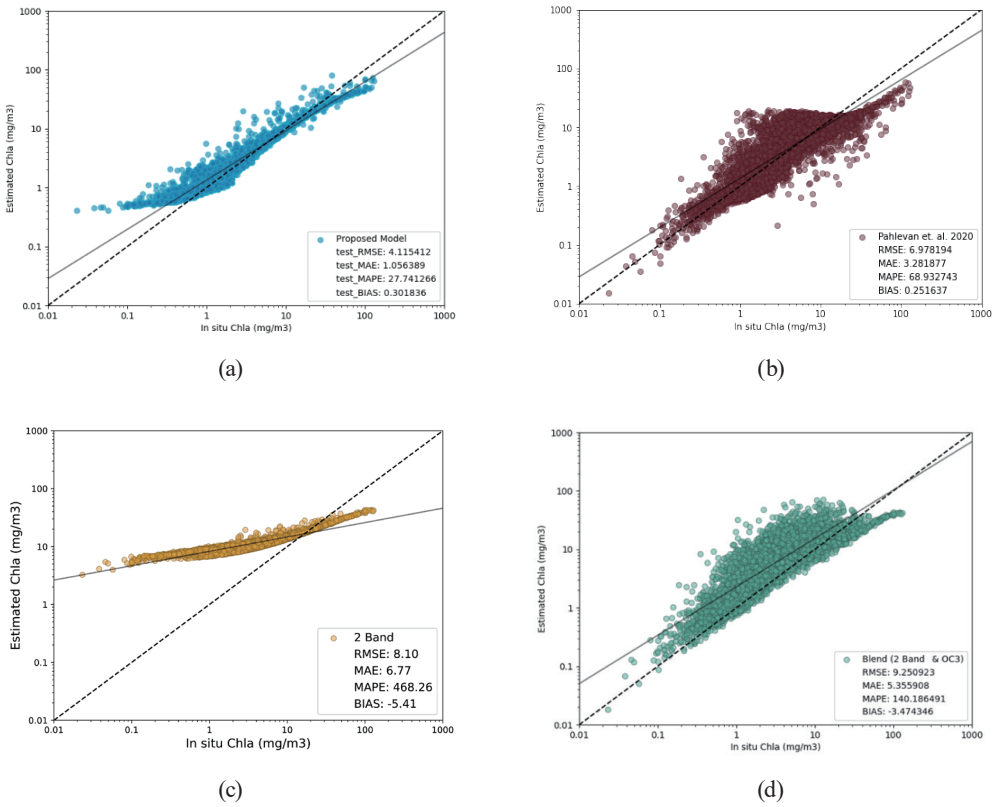

Fig. 7. (Color online) Scatterplots of the top-performing algorithms showing the comparison between the evaluation metrics for the (a) proposed model, (b) MDN model, (c) 2 Band algorithm, and (d) Blend algorithm evaluated on the basis of the simulated dataset.

Table 5
Detailed comparison between the top-performing Chla retrieval algorithms against different Chla ranges based on the simulated dataset.

Chla range (mg/m^3)	Model	*RMSE*	*MAE*	*MAPE*	*BIAS*
0 to 5	Proposed Model	**0.76**	**0.38**	**36.43**	**−0.21**
	MDN	3.30	1.77	83.09	−1.39
	OCI	5.93	3.53	168.99	−3.49
	Blend (2 Band & OC3)	5.93	3.53	169.07	−3.50
5 to 10	Proposed Model	**1.53**	**0.69**	**10.06**	**−0.35**
	MDN	4.12	3.04	45.62	−1.62
	OCI	10.73	7.67	114.38	−7.44
	Blend (2 Band & OC3)	10.73	7.66	114.33	−7.44
10 to 20	Proposed Model	**2.18**	**0.93**	**6.55**	**0.08**
	MDN	4.83	3.94	28.28	3.01
	OCI	12.73	8.06	61.13	−5.57
	Blend (2 Band & OC3)	11.62	7.43	56.95	−5.29
20 to 150	Proposed Model	**16.53**	**10.20**	**21.69**	**8.69**
	MDN	25.10	20.29	52.06	20.29
	OCI	30.78	21.28	50.44	16.31
	Blend (2 Band & OC3)	22.00	15.33	36.48	12.68

Table 6
Overall evaluation for all models based on the *in situ* test dataset.

Model	*RMSE*	*MAE*	*MAPE*	*BIAS*
Proposed Model	**20.05**	**10.00**	**66.89**	**5.54**
MDN	22.58	12.44	72.40	8.92
OC3	32.35	14.98	96.06	8.04
OCI	32.35	14.98	96.06	8.04
2 Band Ratio	21.67	11.30	124.04	1.40
3 Band Ratio	23.21	16.44	223.44	2.94
4 Band Ratio	22.28	15.11	209.01	2.05
Blend (2 Band & OC3)	22.78	11.36	85.68	4.61

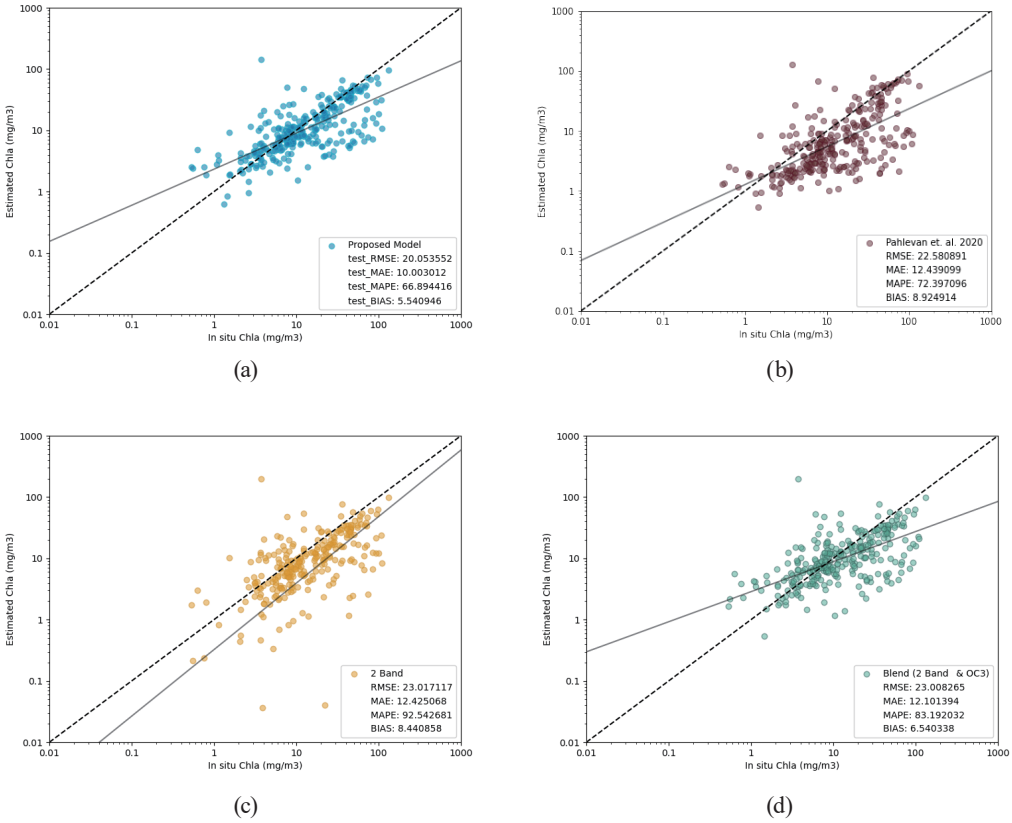

Fig. 8. (Color online) Scatterplots of the top-performing algorithms showing the comparison between the evaluation metrics for (a) the proposed model, (b) MDN model, (c) 2 Band algorithm, and (d) Blend algorithm evaluated on the basis of the *in situ* test dataset.

reduction in *RMSE* and a 21.18–47.34% reduction in *MAE*. Furthermore, the proposed model also excels in higher Chla ranges; in the range of 10–20 mg/m^3, *RMSE* is 23.5% less than that of the MDN model and 23.2–29.27% less than that of the standard algorithms. *MAE* is also reduced by 10.85–36.63% compared with the other models, as reflected in the scatterplots of Fig. 8. The standard algorithms showed better results than the MDN model in this range in terms of *MAE*. Finally, 2 Band performed better than the other models in the highly turbid water Chla range (20–150 mg/m^3).

Table 7
A detailed comparison between the top-performing Chla retrieval algorithms against different ranges of Chla based on the *in situ* test dataset.

Chla range (mg/m^3)	Model	*RMSE*	*MAE*	*MAPE*	*BIAS*
0 to 5	Proposed Model	18.00	4.53	160.42	−4.11
	MDN	**16.11**	**4.00**	**128.74**	**−2.28**
	2 Band Ratio	27.66	9.60	380.02	−8.89
	Blend (2 Band & OC3)	26.88	6.01	206.08	−5.56
5 to 10	Proposed Model	**6.73**	**3.46**	**46.84**	−1.57
	MDN	8.01	4.39	59.17	**1.54**
	2 Band Ratio	9.43	6.57	93.19	−6.48
	Blend (2 Band & OC3)	9.79	4.97	69.27	−3.35
10 to 20	Proposed Model	**7.78**	**5.26**	**37.18**	**1.72**
	MDN	10.17	8.30	59.89	5.91
	2 Band Ratio	10.13	5.90	43.56	−3.68
	Blend (2 Band & OC3)	11.00	6.92	50.36	−0.03
20 to 150	Proposed Model	29.25	19.96	41.23	17.90
	MDN	33.98	24.94	55.45	22.02
	2 Band Ratio	**27.20**	**18.08**	**35.80**	**15.24**
	Blend (2 Band & OC3)	29.76	21.00	44.47	18.23

3.3. Models' performance

In this study, we compared the performance of the proposed 1D CNN model for Chla retrieval with those of six standard algorithms and the MDN model using simulated and *in situ* datasets. The results indicate that the proposed model outperforms the other models, with significant improvements in terms of *RMSE*, *MAE*, and *MAPE*. The results from the simulated dataset showed that the proposed model provided the highest accuracy across various Chla ranges. However, when considering the *in situ* dataset, the proposed model performed best in the mid-Chla range (5 < Chla < 20 mg/m^3). The statistical analysis of the *in situ* dataset highlights the need to improve the accuracy of the proposed model in the future by increasing the size of the trained dataset, particularly for Chla < 1 mg/m^3, which has few samples, as shown in Fig. 3.

The results emphasize that machine-learning-based models, such as the 1D CNN and MDN, consistently outperform the six standard empirical algorithms because they can learn from the trained data, find complex patterns and relationships, automatically extract features from the data, and improve as the dataset size increases, which allows them to detect even more complex relationships in the data. In contrast, standard algorithms rely on predefined equations that may not capture the complexity of the problem. On the other hand, this research proved the applicability of using sequential models to handle Rrs, and that it is more efficient than normal feed forward networks.

4. Conclusion

In this study, we propose a groundbreaking approach for the retrieval of Chla concentrations from different water bodies using satellite imagery and a novel perspective on satellite data in

terms of sequential reflectance values. The algorithm proposed in this research is a 1D convolutional deep neural network that is known to excel in modeling simple sequential data applied to the domain of water quality monitoring to obtain breakthrough results in the retrieval of Chla using Rrs. The proposed model was trained and tested using Rrs–Chla pairs from both simulated and *in situ* data collected using measurements in different water bodies, and was proven to outperform the standard empirical algorithms and state-of-the-art deep learning methods significantly in most cases and Chla ranges. The model excels in the high ranges of Chla (i.e., higher than 5 mg/m^3) with a 7.48–38.02% overall improvement of in *RMSE* and an 11.50–39.17% lower *MAE* than the other algorithms in this study, which proves that using sequence modeling methods such as 1D CNN for Chla concentration retrieval using Rrs is more accurate than using standard algorithms and basic deep learning methods. Limitations of the proposed model lie mainly in the low Chla range performance, which can be mitigated by providing a model with more balanced data between low and high Chla concentrations. Future research could explore the potential of using 1D CNNs for other satellite products, such as total suspended matter or colored dissolved organic matter, and expand the dataset of Rrs–Chla pairs to enhance the robustness of deep learning methods in estimating Chla. Real-time Chla and Rrs measurements can also be used in an online learning manner to further improve the proposed model.

Acknowledgments

The study was partially funded by the Global Change Observation Mission for Climate (GCOM-C) RA7 grant, managed by the Japan Aerospace Exploration Agency (JAXA). We are grateful for the valuable and constructive input given by two anonymous reviewers, which considerably improved the quality and presentation of this manuscript.

Appendix A

The detailed implementations of the standard Chla algorithms are listed below.

OC3:

$$x = \left(\frac{Rrs_{443}}{Rrs_{560}}, \frac{Rrs_{490}}{Rrs_{560}} \right)$$

$$\left(Chla_{OC3} \right) = a_0 + a_1 x + a_2 x^2 + a_3 x^3 + a_4 x^4$$

$$a_0 = 0.3308,\ a_1 = -2.6684,\ a_2 = 1.5990,\ a_3 = 0.5525,\ a_4 = -1.4876$$

CI:

$$CI = Rrs_{560} - Rrs_{443} - \left(\frac{560-443}{665-443} * \left(Rrs_{665} - Rrs_{443} \right) \right)$$

$$\left(Chla_{CI} \right) = -0.4909 + \left(191.6590 * CI \right)$$

OCI (CI & OC3):

$$w = \frac{Chla_{CI} - 0.15}{0.2 - 0.15}$$

$$Chla_{OCI} = \begin{cases} Chla_{CI} & (Chla_{CI} < 0.15) \\ Chla_{OC3} & (Chla_{CI} > 0.2) \\ w * Chla_{OC3} + |w-1| * Chla_{CI} & (\text{otherwise}) \end{cases}$$

2 Band ratio:

$$Chla_{2B} = a_0 + a_1 \frac{Rrs_{705}}{Rrs_{665}}$$

By regression on the datasets used in this study, the parameters for the above linear equation were found to be

$$a_0 = -23.6481638,\ a_1 = 51.54954222.$$

With *RMSE* = 16.66, *MAPE* = 161.93%, R^2 = 0.42.

3 Band ratio:

$$Chla_{3B} = a_0 + a_1 \left[\frac{1}{Rrs_{665}} - \frac{1}{Rrs_{705}} \right] Rrs_{740}$$

By regression on the datasets used in this study, the parameters for the above linear equation were found to be

$$a_0 = 18.19501540, a_1 = -0.00312166.$$

With *RMSE* = 16.18, *MAPE* = 182.43, R^2 = 0.46.

4 Band ratio:

$$Chla_{4B} = a_0 + a_1 \frac{\frac{1}{Rrs_{560}} - \frac{1}{Rrs_{665}}}{\frac{1}{Rrs_{740}} - \frac{1}{Rrs_{705}}}$$

By regression on the datasets used in this study, the parameters for the above linear equation were found to be

$$a_0 = 6.0385872814,\ a_1 = -72.97858459.$$

With $RMSE = 20.33$, $MAPE = 312.17$, $R^2 = 0.14$.

Blend (2 Band & OC3):

$$r = \frac{Rrs_{705}}{Rrs_{665}}$$

$$\varnothing = \begin{cases} 0.75 & r < 0.75 \\ 1.15 & r > 1.15 \\ r & \text{otherwise} \end{cases}$$

$$w = \frac{\varnothing - 0.75}{1.15 - 0.75}$$

$$Chla = w * Chla_{2B} + |w - 1| * Chla_{OC3}$$

References

1 R. E. Carlson: Limnol. Oceanogr. **22** (1977) 361. https://doi.org/10.4319/lo.1977.22.2.0361
2 J. Bartram, I. Chorus, Eds. Toxic Cyanobacteria in Water [Internet]. (CRC Press, 1999) 1st ed.. https://doi.org/10.1201/9781482295061
3 P. C. Golnick, J. D. Chaffin, T. B. Bridgeman, B. C. Zellner, and V. E. Simons: J. Great Lakes Res. **42** (2016) 965. https://doi.org/10.1016/j.jglr.2016.07.031
4 S. C. J. Palmer, T. Kutser, and P. D. Hunter: Remote Sens. Environ. **157** (2015) 1. https://doi.org/10.1016/j.rse.2014.09.021
5 H. J. Gons: Environ. Sci. Technol. **33** (1999) 1127. https://doi.org/10.1021/es9809657
6 K. H. Mittenzwey, S. Ullrich, A. A. Gitelson, and K. Y. Kondratiev: Limnol. Oceanogr. **37** (1992) 147. Available from: https://doi.org/10.4319/lo.1992.37.1.0147
7 J. E. O'Reilly, S. Maritorena, B. G. Mitchell, D. A. Siegel, K. L. Carder, S. A. Garver, M. Kahru, and C. mcClain: J. Geophys. Res. Oceans. **103** (1998) 24937. https://doi.org/10.1029/98JC02160
8 J. E. O'Reilly, and P. J. Werdell: Remote Sens. Environ. **229** (2019) 32. https://doi.org/10.1016/j.rse.2019.04.021

9 J. E. O'Reilly: SeaWiFS postlaunch calibration and validation analyses **11** (2000) 9.
10 C. Hu, Z. Lee, and B. Franz: J. Geophys. Res. Oceans **117** (2012). https://doi.org/10.1029/2011JC007395
11 A. A. Gilerson, A. A. Gitelson, J. Zhou, D. Gurlin, W. Moses, I. Ioannou, and S. A. Ahmed: Opt. Express **18** (2010) 24109. https://doi.org/10.1364/OE.18.024109
12 M. E. Smith, L. R. Lain, and S. Bernard: Remote Sens. Environ. **215** (2018) 217. https://doi.org/10.1016/j.rse.2018.06.002
13 H. Zhan, P. Shi, and C. Chen: IEEE Trans. Geosci. Remote Sens. **41** (2003) 2947. https://doi.org/10.1109/TGRS.2003.819870
14 L. S. Kupssinskü, T. T. Guimarães, E. M. Souza, D. C. Zanotta, M. R. Veronez, L. Gonzaga, F. F. Mauad: Sensors **20** (2020) 2125. https://doi.org/10.3390/s20072125
15 R. Matarrese, A. Morea, K. Tijani, V. Pasquale, M. T. Chiaradia, and G. Pasquariello: 2008 IEEE Int. Geoscience and Remote Sensing Symposium **4** (2008) 910. https://doi.org/10.1109/IGARSS.2008.4779871
16 P. M. Maier, and S. Kelle: Ann. Photogramm. Remote Sens. Spatial Inf. Sci. **IV-2/W5** (2019) 609. https://doi.org/10.5194/isprs-annals-IV-2-W5-609-2019
17 D. Diouf, and D. Seck: IJAIA. **10** (2019) 33. https://doi.org/10.5121/ijaia.2019.10603
18 S. Graban, G. Dall'Olmo, S. Goult, and R. Sauzède: Opt. Express **28** (2020) 24214. https://doi.org/10.1364/OE.397863
19 D. Gómez, P. Salvador, J. Sanz, and J. L. Casanova: Environ. Pollut. **286** (2021) 117489. https://doi.org/10.1016/j.envpol.2021.117489
20 D. Jin, E. Lee, K. Kwon, and T. Kim: Remote Sens. **13** (2021) 2003. https://doi.org/10.3390/rs13102003
21 N. Pahlevan, B. Smith, K. Alikas, J. Anstee, C. Barbosa, C. Binding, M. Bresciani, B. Cremella, C. Giardino, D. Gurlin, V. Fernandez, C. Jamet, K. Kangro, M. K. Lehmann, H. Loisel, B. Matsushita, N. Hà, L. Olmanson, G. Potvin, S. G. H. Simis, A. VanderWoude, V. Vantrepotte, and A. Ruiz-Verdù: Remote Sens. Environ. **270** (2022) 112860. https://doi.org/10.1016/j.rse.2021.112860
22 B. Smith, N. Pahlevan, J. Schalles, S. Ruberg, R. Errera, R. Ma, C. Giardino, M. Bresciani, C. Barbosa, T. Moore, V. Fernandez, K. Alikas, and K. Kangro: Front. Remote Sens. **1** (2021). https://doi.org/10.3389/frsen.2020.623678
23 N. Pahlevan, B. Smith, J. Schalles, C. Binding, Z. Cao, R. Ma, K. Alikas, K. Kangro, D. Gurlin, N. Hà, B. Matsushita, W. Moses, S. Greb, M. K. Lehmann, M. Ondrusek, N. Oppelt, and R. Stumpf: Remote Sens. Environ. **240** (2020) 111604. https://doi.org/10.1016/j.rse.2019.111604
24 S. Kiranyaz, T. Ince, R. Hamila, and M. Gabbouj: 37th Ann. Int. Conf. the IEEE Engineering in Medicine and Biology Society (EMBC, 2015) 2608. https://doi.org/10.1109/EMBC.2015.7318926
25 S. Salem, H. Higa, H. Kim, H. Kobayashi, K. Oki, and T. Oki: Sensors **17** (2017) 1746. https://doi.org/10.3390/s17081746
26 B. Nechad, K. Ruddick, T. Schroeder, K. Oubelkheir, D. Blondeau-Patissier, N. Cherukuru, V. Brando, A. Dekker, L. Clementson, A. C. Banks, S. Maritorena, P. J. Werdell, C. Sá, V. Brotas, I. Caballero de Frutos, Y. H. Ahn, S. Salama, G. Tilstone, V. Martinez-Vicente, D. Foley, M. McKibben, J. Nahorniak, T. Peterson, A. Siliò-Calzada, R. Röttgers, Z. Lee, M. Peters, and C. Brockmann: Earth Syst. Sci. Data **7** (2015) 319. https://doi.org/10.5194/essd-7-319-2015
27 M. Drusch, U. del Bello, S. Carlier, O. Colin, V. Fernandez, F. Gascon, B. Hoersch, C. Isola, P. Laberinti, P. Martimort, A. Meygret, F. Spoto, O. Sy, F. Marchese, and P. Bargellini: Remote Sens. Environ. **120** (2012) 25. https://doi.org/10.1016/j.rse.2011.11.026
28 S. Kiranyaz, O. Avci, O. Abdeljaber, T. Ince, M. Gabbouj, and D. J. Inman: Mech. Syst. Signal Process. **151** (2021) 107398. https://doi.org/10.1016/j.ymssp.2020.107398
29 F. T. Liu, K. M. Ting, and Z. H. Zhou: Eighth IEEE Int. Conf. Data Mining (2008) 413. https://doi.org/10.1109/ICDM.2008.17
30 G. Dall'Olmo, A. A. Gitelson, and D. C. Rundquist: Geophys. Res. Lett. **30** (2003). https://doi.org/10.1029/2003GL018065
31 C. Le, Y. Li, Y. Zha, D. Sun, C. Huang, and H. Lu: Remote Sens. Environ. **113** (2009) 1175. https://doi.org/10.1016/j.rse.2009.02.005

About the Authors

Muhammad Salah is a master's student at the School of Engineering at Kyoto University of Advanced Science, expected to graduate in September 2024. Also working as a teaching assistant in the Department of Electrical and Mechanical Systems Engineering at Kyoto University of Advanced Science since 2022. Earned his B.Sc. in Computer and Systems Engineering from Alexandria University in 2021. His main research interests include utilizing deep learning methods for water quality monitoring, generative methods in deep learning, and sequential analysis and modeling of data.

Hiroto Higa earned his Ph.D. in Environmental Studies from The University of Tokyo, Japan, in 2015. He earned his B.Sc. in Civil Engineering from Tokyo University of Science, Japan, in 2010, and his M.Sc. in Environmental Studies from The University of Tokyo, Japan, in 2012. Higa served as a Special Researcher at the Japan Society for the Promotion of Science from 2015 to 2016. From 2016 to 2021, he held the position of assistant professor at Yokohama National University. Since 2022, Higa has been serving as an associate professor at the Institute of Urban Innovation, Yokohama National University, Japan. Additionally, he acts as an ad-hoc reviewer for several international journals. Higa's research primarily focuses on coastal environmental engineering studies and ocean color remote sensing for turbid water areas.

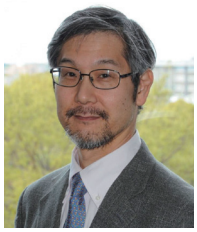

Joji Ishizaka earned his Ph.D. in Geoscience from Texas A&M University, US, in 1989. He received his B.Sc. in Biology and M.Sc. in Environmental Studies, Tsukuba University, Japan, in 1981 and 1983, respectively. Ishizaka served as a Research Scientist at the Agency of Industrial Sciences and Technology, Ministry of International Trade and Industry, for 11 years (1989–1998). From 1998 to 2009, he worked as a professor at Faculty of Fisheries, Nagasaki University, Japan. From 2009 to 2015, Ishizaka worked as a professor at the Hydrospheric-Atomspheric Research Center, Nagoya University, Japan, and also served as the director of the center in 2013–2015. Since 2015, he worked as a professor at the Institute for Space-Earth Environmental Reseach, Nagoya University, and served as the vice director of the institute in 2015 to 2019. Ishizaka's research focus on the variation of phytoplankton and primary production associated with natural and anthropogenic effects using ocean color remote sensing.

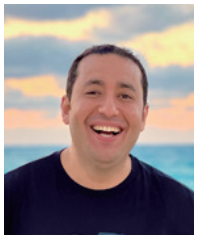

Salem Ibrahim Salem earned his Ph.D. in Civil Engineering from The University of Tokyo, Japan, in 2017. He received his B.Sc. and M.Sc. in Civil Engineering from Alexandria University, Egypt, in 2005 and 2011, respectively. Salem served as a full-time teaching assistant at the School of Engineering, Alexandria University, for eight years (2006–2014). From 2017 to 2019, he held a postdoctoral researcher position at The University of Tokyo. Since 2019, Salem has been working as a junior associate professor at the Faculty of Engineering, Kyoto University of Advanced Science, Kyoto, Japan. He also acts as an ad-hoc reviewer for several international journals. Salem's research primarily centers on remote sensing for water resources and environmental studies, integrating the latest advances in machine learning into his work.